Desalination and Water Treatment
www.deswater.com

doi:10.5004/dwt.2017.0372

69 (2017) 268–283
March

Heterogeneous catalytic degradation of phenol by a Fenton-type reaction using copper ferrites ($CuFe_2O_4$)

Najwa Hamdan[a], Mohammad Abu Haija[a,*], Fawzi Banat[b], Asma Eskhan[b]

[a]*Department of Chemistry,, The Petroleum Institute, PO Box 2533, Abu Dhabi, UAE, emails: joojoo400@gmail.com (N. Hamdan), mabuhaija@pi.ac.ae (M. Abu Haija)*
[b]*Department of Chemical Engineering, The Petroleum Institute, PO Box 2533, Abu Dhabi, UAE, email: aeskhan@pi.ac.ae (A. Eskhan), fbanat@pi.ac.ae (F. Banat)*

Received 4 April 2016; Accepted 25 July 2016

ABSTRACT

The potential application of copper ferrite ($CuFe_2O_4$) as a heterogeneous catalyst in the process of phenol degradation was investigated using high performance liquid chromatography (HPLC). $CuFe_2O_4$ nanoparticles were synthesized by sol-gel auto combustion and co-precipitation methods, and subsequently were calcined at 500°C and 750°C. The prepared ferrites were characterized for their morphology, crystallinity, purity, and stability using various techniques such as X-ray diffraction (XRD), infrared spectroscopy (IR), scanning electron microscopy (SEM), transmission electron microscopy (TEM), thermogravimetric analysis (TGA), and BET surface area analysis. The sol-gel derived $CuFe_2O_4$ particles exhibited spinel phases of higher porosity and crystallinity as well as higher catalytic activity toward the degradation of phenol. Calcination of $CuFe_2O_4$ resulted in larger particles of higher purity and crystallinity, but of lower catalytic activity towards the degradation of phenol. The catalytic activity of the sol-gel $CuFe_2O_4$ was compared with the activity of two other sol-gel prepared ferrite catalysts, zinc ferrite ($ZnFe_2O_4$) and magnesium ferrite ($MgFe_2O_4$) catalysts, and with a commercial titanium dioxide (TiO_2) catalyst. Among these catalysts, HPLC results demonstrated that $CuFe_2O_4$ exhibited the highest catalytic activity towards the degradation of phenol. Furthermore, the effects of several experimental parameters on the degradation rate of phenol over $CuFe_2O_4$ were investigated including the solution pH, reaction temperature, H_2O_2 concentration, catalyst loading, H_2O_2 addition mode, stirring, and the presence of UV or sunlight radiations. The degradation rate was enhanced by increasing the H_2O_2 concentrations, the $CuFe_2O_4$ catalyst loadings, or the reaction temperature. A faster and complete removal of phenol was observed under acidic conditions or under the presence of UV or sunlight radiation. $CuFe_2O_4$ was successfully regenerated and reused for five degradation cycles without noticeable loss in its activity.

Keywords: Phenol degradation; Fenton; Copper ferrites

1. Introduction

Since the beginning of the industrial revolution, different types of pollutants have been introduced to the environment. Among these pollutants, phenol is reported as a refractory pollutant presents in the wastewater discharges of various industries including petroleum refining, petrochemical, plastic, polymer, fiberglass, cosmetics, pharmaceutical, paints, dyes, leather, adhesives, smelting and metallurgical industries [1]. Due to its highly toxic, carcinogenic and endocrine disrupting properties, strict standards have been placed to control phenol discharges into the water bodies [2,3]. Phenol and its derivatives constitute the 11th in the 126 chemicals list designated as the primary pollutants by the Environmental Protection Agency (EPA) in the USA [1]. The

*Corresponding author.

Presented at the EDS conference on Desalination for the Environment: Clean Water and Energy, Rome, Italy, 22–26 May 2016.

EPA has set a limit of 0.1 ppm for phenol levels in the wastewater discharges [1]. Consequently, several techniques have been developed to remove phenol from industrial wastewaters which can be divided into biological degradation [4] and other physico-chemical separation processes including flocculation [5], adsorption [6] and separation membranes [7]. The biodegradation processes are adequate for low concentrations of phenol, around 50 ppm or lower, and they are relatively slow which does not allow for high degrees of removal [3,8]. The classical physico-chemical separation processes, on the other hand, involve the transfer of phenol into another phase which in turn requires a post-treatment process [3,9]. An alternative promising method is the catalytic advanced oxidation processes (AOPs) which degrade a variety of organic pollutants.

The AOPs are chemical methods based on the generation of active free radicals, such as hydroxyl radicals (HO•). The highly active, non-selective hydroxyl radicals are able to react with all classes of organic pollutants, resulting in complete mineralization to carbon dioxide and water [9,10]. Hydrogen peroxide (H_2O_2) is widely used as an effective source of free hydroxyl radicals due to its complete solubility in water which eliminates mass transfer resistances [3]. Moreover, H_2O_2 is an ecological reactant that does not form any toxic by-products [3]. However, to enhance the decomposition of hydrogen peroxide to free hydroxyl radicals, a source of energy or a catalytic system (homogeneous or heterogeneous) is needful. The system which consists of hydrogen peroxide in conjunction with iron (II) ions in water solution is called Fenton's reagent [3]. The generation of hydroxyl radicals from hydrogen peroxide in a Fenton-type system occurs according to the following reaction [3]:

$$H_2O_2 + Fe^{2+} \rightarrow Fe^{3+}HO\cdot + OH \quad (1)$$

Fenton-type reactions can be employed to treat a variety of wastewaters containing different hazardous pollutants such as phenols, pesticides, formaldehydes and plastic additives [11]. However, homogeneous Fenton systems are highly pH sensitive and produce large volumes of chemical wastes which need further treatments [1,3]. Therefore, different heterogeneous Fenton catalysts have been developed to treat wastewater.

Spinel ferrites are metal oxides which widely used in various applications due to their unique phsico-chemical and electrical properties. They are also used as catalysts in removing organic pollutants [12,13]. For example, Liu et al. has used nickel ferrites ($NiFe_2O_4$) synthesized by the hydrothermal method for the degradation of rhodamine B in the presence of oxalic acid [14]. Moreover, Nivethitha et al. has used zinc and cobalt ferrite nanoparticles for the degradation of methylene blue, crystal violet and alizarin red dyes. Spinel ferrites have the general formula of MFe_2O_4, where M^{2+} represents a divalent metallic ion such as Fe^{2+}, Mn^{2+}, Ni^{2+}, Co^{2+}, and Cu^{2+}. The spinel ferrite unit cell consists of a face centered cubic lattice of oxygen ions, with the M^{2+} and Fe^{3+} ions located in the tetrahedral and octahedral sites of the lattice [15]. The catalytic properties of the spinel ferrites depend on the redox properties of the transition metal ions (M^{2+}) and their distribution among the octahedral and tetrahedral sites [15]. In addition, the synthesis method and the particle size of the catalyst play a role in determining its catalytic activity [15]. Different methods have been suggested to prepare spinel ferrite nanoparticles including combustion, microwave, sol-gel, co-precipitation and solid-state reactions [12]. The sol-gel and co-precipitation methods are the most well-known techniques for preparing ferrites. The advantages of these preparation methods are the high productivity, simplicity, clean and green synthesis, and commercially feasible work-up procedures [16]. The sol-gel method creates porous nanoparticles after a thermal reaction between metal nitrates and a reducing agent such as citric acid. Typically, the preparation procedure involves dissolving the metal nitrates and the reducing agent in water, stirring and heating until water evaporates and finally forming a gel. Further heating above 250°C causes exothermic combustion and a rapid evolution of heat. This creates high crystallinity ferrites with open pore structures [17]. The co-precipitation method is a low-temperature preparation method for precipitating nanoparticles from metal salt aqueous solutions. Due to the low preparation temperature of the co-precipitation method, the prepared ferrites are usually of low crystallinity with additional amorphous impurity phases. Therefore, additional annealing at temperatures above 500°C is necessary to increase the phase purity and crystallinity [18].

Among various ferrites, $CuFe_2O_4$ has many distinctive features, and therefore, it is used in different applications. It showed high reactivity, chemical stability, and durability in catalytic processes [19–21]. It was used in photocatalytic degradation of methylene blue [22] as well as in converting CO to CO_2 [23]. Further, $CuFe_2O_4$ was applied to initiate the fabrication of 1,4-dihydropyridines, β, γ-unsaturated ketones [24] and α-aminonitriles [25]. In the present work, the application of $CuFe_2O_4$ as a catalyst for phenol remediation was investigated. The $CuFe_2O_4$ powders were prepared by sol-gel auto combustion and co-precipitation methods, and were characterized by different techniques such as X-ray diffraction (XRD), IR, TGA, SEM, TEM and BET surface area analysis. The prepared $CuFe_2O_4$ catalysts were then subjected to heat treatment at 500°C and 750°C. The catalytic activities of the $CuFe_2O_4$ catalysts, prepared via different methods and at different calcination temperatures, towards the degradation of phenol were investigated and compared. Two other ferrite catalysts, $ZnFe_2O_4$ and $MgFe_2O_4$, were also prepared and compared to $CuFe_2O_4$ catalyst. A commercial TiO_2 catalyst was also used for comparison purposes. The influences of several experimental conditions on the removal of phenol were investigated, such as the solution pH, reaction temperature, catalyst loading, H_2O_2 concentration, H_2O_2 addition mode, stirring, and the presence of UV or sunlight radiation.

2. Materials and methods

2.1. Catalysts preparation

The main catalyst used in this work, copper ferrite ($CuFe_2O_4$), was prepared by two different methods, namely the sol-gel auto combustion and the co-precipitation methods. Two other ferrite catalysts ($MgFe_2O_4$ and $ZnFe_2O4$) were also prepared via the sol-gel method for the purpose of comparison. Additional comparative studies were carried out using TiO_2 (>99%) which was purchased from Sigma-Aldrich and was used as received.

In the sol-gel method, the different catalysts were prepared by mixing a stoichiometric amount of ferric nitrate powder ($Fe(NO_3)_3.9H_2O$) with the corresponding metal nitrate salts ($Cu(NO_3)_2.3H_2O$, $Mg(NO_3)_2.6H_2O$ or $Zn(NO_3)_2.6H_2O$) in measured volumes of distilled water. Citric acid was then added to form a homogeneous solution. The molar ratio of the ferric nitrate to metal nitrate to citric acid was 2:1:3. The solution was heated up to 80°C using a hot plate with continuous magnetic stirring. Then ammonium hydroxide solution was added to the solution to adjust the pH value to 8. The obtained mixture was evaporated at about 100°C until it became viscous. The mixture was kept overnight at room temperature to obtain a highly viscous gel which was then heated using a hot plate to initiate a self-propagating combustion reaction accompanied with vigorous evolution of gases. The resulting ash-like powder was crushed and grinded to form a very fine powder. Hereafter, this powder is referred to as "as-prepared$CuFe_2O_4$". Thermal treatments for the as-prepared samples were carried out at temperatures of 500°C and 750°C in air for 5 h.

In the co-precipitation method, copper ferrite catalysts were prepared by two different procedures. In the first procedure, a solution of $Fe(NO_3)_3.9H_2O$ and $Cu(NO_3)_2.3H_2O$ was prepared in a ratio of 2:1 with continuous stirring followed by rising the temperature to 60°C. In order to adjust the solution pH in the range of 10–12, drops of 5 M NaOH solution was added slowly to the solution and then cooled down to room temperature. The precipitate was filtered and washed well with distilled water, and then dried in an oven at 120°C. The second procedure was carried out by mixing 0.05 mole $Fe(NO_3)_3.9H_2O$ with 0.025 mole $Cu(NO_3)_2.3H_2O$ in 100 ml distilled water. Afterward, 75 ml of 4 M NaOH were added to the solution and then heated up to 90°C for 2 h with stirring. The precipitate was filtered and washed well with distilled water, and then dried in an oven at 120°C. All the obtained as-prepared powders from the above-mentioned two co-precipitation procedures were further subjected to heat treatments at 500°C and 750°C in air for 5 h.

2.2. Catalysts characterization

The different as-prepared and calcined catalyst samples were characterized by X-ray diffractometer to determine the quality, identity, structure, phase transition, purity, and crystallite size of the catalysts. XRD data were collected by PANalytical Powder Diffractometer (X'Pert PRO) using Cu-Ka radiation (λ = 1.5406 Å, 40 kV, 40 mA). Diffraction patterns were collected in the 2θ range of 10°–80°, with a step size of 0.02°. The crystallite sizes of the analyzed catalysts was obtained using the Debye-Scherrer formula [26]:

$$L = \frac{K\lambda}{B\cos\theta} \tag{2}$$

where K is the Scherrer's constant and is equal to 0.9, λ is the wavelength in nm used in the XRD instrument, B is the peak width at half maximum, θ is the diffraction angle and L is the crystallite size in nm.

The morphologies of the ferrite powders were visualized using scanning electron microscopy (SEM). The SEM measurements were carried out using FEG QUANTA 250 operating at 30 kV. Transmission electron microscopy (TEM) images for all the prepared ferrite catalysts were obtained by FEI Tecnai 20 with an accelerating voltage of 200 kV. The ferrite powders were also characterized by Nicolet iS10 FT-IR spectrometer, using a KBr pelletat room temperature with a spectral range of 400–4,000 cm^{-1}. Thermogravimetric analysis (TGA) was conducted to determine the weight loss percentage in ~10 mg of the as-prepared ferrite powder as a function of temperature. The process was accomplished when the measured sample was heated up to 750°C in nitrogen with a heating rate of 15°C/min. BET surface analyzer (Quanta chrome, Autosorb 06) was used to determine the specific surface area, pore size and pore volume of the ferrites. N_2 physisorption was carried out at liquid N_2 temperature (77 K), and the surface area was calculated using the BET method.

2.3. Phenol degradation experiments

Different experiments were designed and performed to investigate the catalytic activity of the prepared ferrite catalysts toward the degradation of phenol in water. In a typical experiment, the reaction was carried out in an open 250 conical flask containing 100 mL of 200 ppm phenol solution and a pre-determined volume of 30% H_2O_2. Unless otherwise mentioned, 30 mg of a catalyst were added to the mixture which was kept at the room temperature with continuous stirring. Samples were withdrawn every 30 min and immediately filtered using a 0.2-μm nylon membrane filters to remove the suspended catalyst particles. The filtrate was directly analyzed for phenol concentration using high pressure liquid chromatography (HPLC, Shimadzu) equipped with a UV detector which was set at 280 nm. The mobile phase was composed of a mixture of methanol, water, and acetic acid in a percentage ratio of 35:64:1, respectively. Volumes of 10 μL of the filtrate were injected via an auto sampler through a C18 column (Restek, 150 × 4.6 mm) at a flow rate of 1 mL/min.

The applied HPLC method was accurate and suitable for tracing the phenol degradation process. The identification of the reaction intermediate products, such as hydroquinone and catechol, was also accomplished by the same HPLC method. From environmental point of view, the removal of such intermediates from wastewater is an important concern since they are as harmful as phenol. It is worth mentioning that in this work and based on the HPLC results, complete removal of phenol and its intermediates was achieved under the following reaction conditions: increasing the reaction time, increasing the reaction temperature, increasing the H_2O_2 concentration, lowering the pH of the reaction solution, or exposing the reaction to UV or sunlight radiation.

The degradation efficiency of the catalyst was calculated by applying the following equation:

$$\text{Degradation}\,\% = \frac{(C_0 - C_t)}{C_0} \times 100 \tag{3}$$

where C_0 is the initial phenol concentration and C_t is the residual phenol concentration in the solution at a given time.

The degradation process of phenol was modeled using the following first-order integrated expression [2]:

$$\ln\left(\frac{C}{C_0}\right) = -Kt \tag{4}$$

where C is the residual phenol concentration in the solution in ppm, k is the reaction rate coefficient, t is the time in minutes, and C_0 is the initial concentration of phenol in ppm. The rate constant (k) can be calculated from the slope of $\ln(C/C_0)$ vs. time.

Moreover, the activation energy of the phenol degradation reaction was determined using Arrhenius equation [2]:

$$k = A\, e^{-\frac{E_a}{RT}} \tag{5}$$

where k is the reaction rate constant, A is the pre-exponential factor, E_a is the activation energy, R is the gas constant, and T is the temperature. The activation energy can be calculated by substituting two rate constants and the two corresponding reaction temperatures into the equation:

$$\ln\frac{k_1}{k_2} = \frac{-E_a}{R}\left(\frac{1}{T_1} - \frac{1}{T_2}\right) \tag{6}$$

where $k_1$and k_2 are the reaction rate constants at temperatures T_1 and T_2, respectively.

3. Results and discussion

3.1. Catalysts characterization

3.1.1. XRD characterization

XRD measurements were performed for all the as-prepared and calcined ferrites which were synthesized via the sol-gel and co-precipitation methods. Fig. 1(A) shows the XRD patterns of the sol-gel, as-prepared $CuFe_2O_4$ sample. The XRD pattern of the as-prepared sample is in agreement with the data for standard $CuFe_2O_4$ (JCPDS card 77–0,010), and with literature reports [27–29]. The observed reflection from planes (111), (220), (311), (222), (400), (422), (511), (440), and (533) for the sol-gel, as-prepared $CuFe_2O_4$ confirms that the $CuFe_2O_4$ was made up of mostly pure crystallites of spinel ferrite with a cubic phase [30]. The XRD patterns of the other sol-gel, as-prepared $ZnFe_2O_4$ and $MgFe_2O_4$ are illustrated in Fig. 1(B), and they are matching the diffracted peaks in JCPDS cards 79–1,150 and 71–1,232, respectively, and in agreement with literature reports [31–33].

The effect of calcination on the phase structure of the sol-gel, as-prepared $CuFe_2O_4$ is clear in Fig. 1(C). Starting with a cubic structure of the as-prepared sample, calcination at 500°C or 750°C results in a transition to the tetragonal phase of $CuFe_2O_4$ [34]. The reflections on the tetragonal crystal lattices are (101), (112), (200), (103), (211), (202), (004), (220), (312), (105), (303), (321), (224), (400), (413), (422) and (404). Moreover, increasing the temperature is expected to increase the size of the crystallites [35]. In order to evaluate such increment, the crystallite size was calculated using Eq. (2) and found to be 27 and 32 nm for as-prepared and calcined sol-gel derived samples, respectively.

Fig. 1(D) represents the diffraction patterns of $CuFe_2O_4$ prepared by co-precipitation methods I and II. Comparing the XRD patterns in Figs 1(A) and (D) indicates that the $CuFe_2O_4$ prepared by the sol-gel method is of higher purity and crystallinity. The XRD patterns of the sol-gel derived samples show all the distinctive peaks that confirm the presence of cubic or tetragonal ferrite phases. However, the situation is different for the samples prepared by co-precipitation methods I and II. The diffractograms of these samples indicate the presence of other iron and copper oxides in the samples.

The XRD patterns suggest that the formation of spinel $CuFe_2O_4$ is enhanced by increasing the calcination temperature to 750°C. This is more obvious from XRD results of the sol-gel samples (Fig. 1(C)) which suggest that the calcination may promote the solid-state reaction [36]:

$$CuO + Fe_2O_3 \rightarrow CuF_2O_4 \tag{7}$$

3.1.2. FTIR characterization

Ferrites are known to have two vibrational modes which are related to the variations of the cations and the oxygen ions in two different sublattices. The highest frequency mode ν_1 at ~600 cm^{-1} is related to the stretching vibration of iron-oxygen ions in tetrahedral sites, while the lowest absorption band ν_2 at ~400 cm^{-1} is related to stretching vibration of metal-oxygen ions in octahedral sites [37]. There are several factors that affect the position of the peaks in the IR spectrum such as concentration and mass of the prepared metal oxide, the distance between the cations and oxygen, and the bonding forces [38]. The variations in the absorption bands among the prepared ferrites, as depicted in Fig. 2, can be attributed to the change in the distance of metal-oxygen bonds in the tetrahedral and octahedral sites, and to the type of the metal Cu, Zn, or Mg [39]. The values of the highest frequency characteristic peak ν_1 of the prepared ferrites are summarized in Table 1.

The observation of additional absorption peaks in the range of 1,000–1,750 cm^{-1} for the co-precipitation derived samples may suggest incomplete chemical reactions or complexation processes between metal ions. However, similar IR spectra were observed for ferrites in the literature [40–43]. The peaks at around 1,640 and 3,500 cm^{-1} are attributed to HO bending mode and stretching mode of H_2O molecules, respectively [37,44].

3.1.3. TGA characterization

The thermal stability of the as-prepared, sol-gel and co-precipitation ferrite samples at elevated temperatures was investigated by TGA. The TGA curves of the different prepared ferrites are presented in Fig. 3, which show the mass losses in the temperature range between 25°C and 750°C. The total weight loss of each sample prepared by the sol-gel method, $CuFe_2O_4$, $MgFe_2O_4$ or $ZnFe_2O_4$, was about 2%. The surface water molecules can be expected to evaporate when the temperature reached about 120°C, after which subsequent decomposition of hydroxides, oxides or organic residuals may occur. Above 500°C, no loss in weight was detected which suggested the generation of stable ferrite phases [32,45].

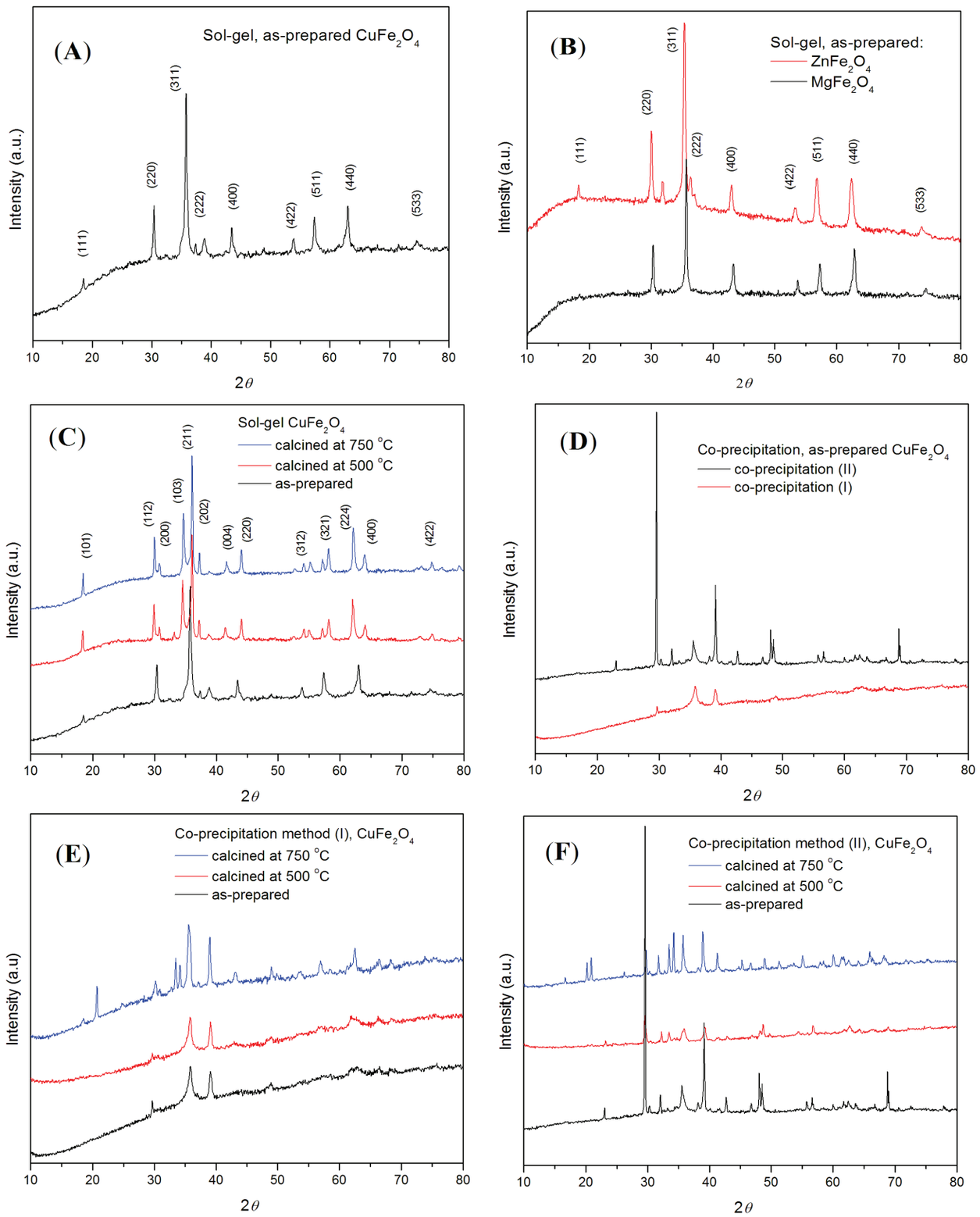

Fig. 1. XRD patterns of ferrite samples: (A) Sol-gel, as-prepared $CuFe_2O_4$, (B) sol-gel method: as-prepared $ZnFe_2O_4$and as-prepared $MgFe_2O_4$, (C) sol-gel, $CuFe_2O_4$ samples: as-prepared, calcined at 500°C, and calcined at 750°C, (D) as-prepared $CuFe_2O_4$ by co-precipitation methods I and II, (E) co-precipitation method I, $CuFe_2O_4$ samples: as-prepared, calcined at 500°C, and calcined at 750°C, (F) co-precipitation method II, $CuFe_2O_4$ samples: as-prepared, calcined at 500°C, and calcined at 750°C.

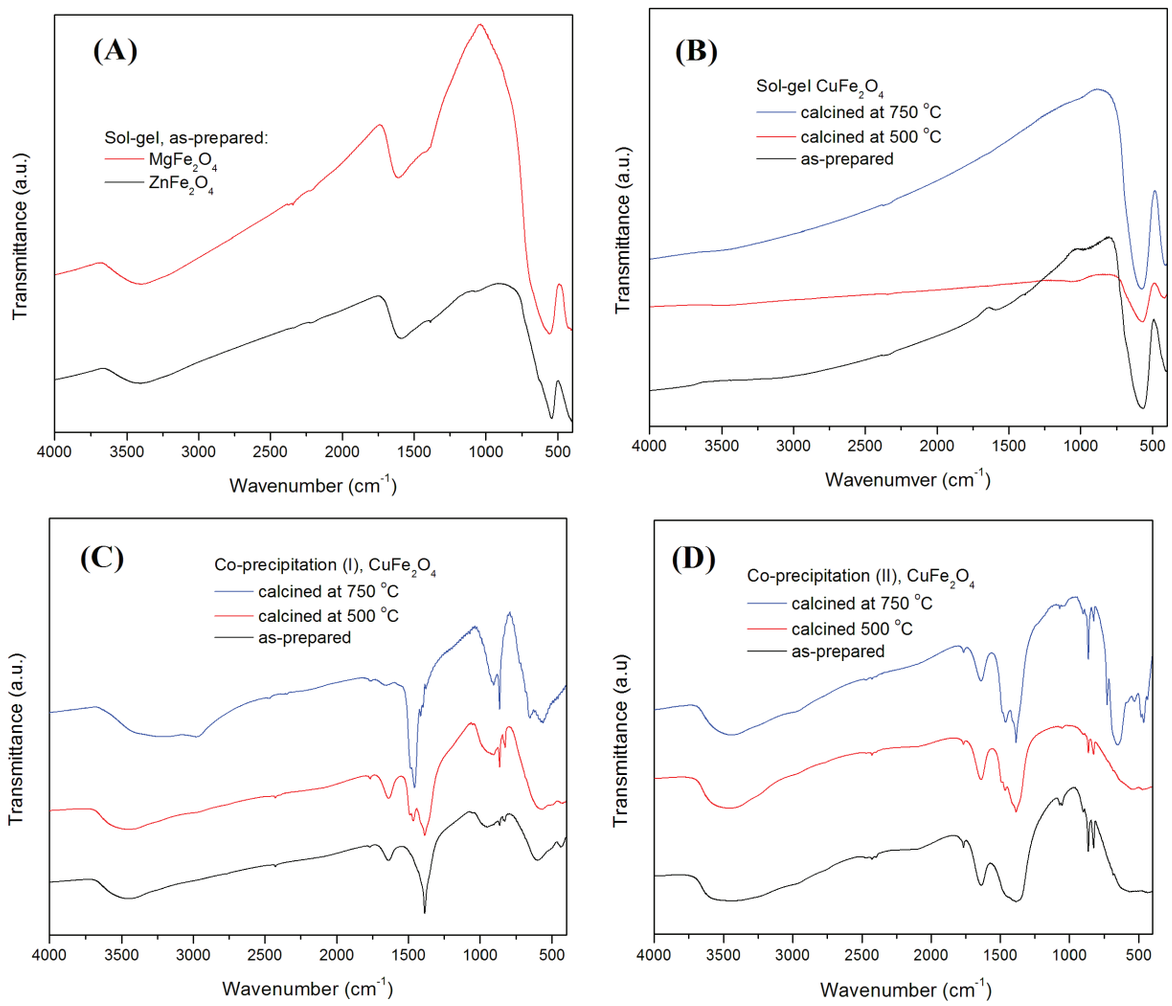

Fig. 2. FTIR spectra of ferrite samples: (A) sol-gel method: as-prepared $ZnFe_2O_4$ and as-prepared $MgFe_2O_4$, (B) sol-gel; $CuFe_2O_4$ samples: as-prepared, calcined at 500°C, and calcined at 750°C, (C) co-precipitation method I; $CuFe_2O_4$ samples: as-prepared, calcined at 500°C, and calcined at 750°C, (D) co-precipitation method II; $CuFe_2O_4$ samples: as-prepared, calcined at 500°C, and calcined at 750°C.

Table 1
The characteristic IR absorption band for the Zn, Mg, and Cu ferrites prepared by various methods and annealed at different temperatures

Type of sample	V_i (cm^{-1})
Sol-gel, as-prepared $CuFe_2O_4$	577
Sol-gel $CuFe_2O_4$ calcined at 500°C	571
Sol-gel $CuFe_2O_4$ calcined at 750°C	575
Co-precipitaion I, as-prepared $CuFe_2O_4$	599
Co-precipitaion I, $CuFe_2O_4$ calcined at 500°C	572
Co-precipitaion I, $CuFe_2O_4$ calcined at 750°C	562
Co-precipitaion II, as-prepared $CuFe_2O_4$	Not detected
Co-precipitaion II, $CuFe_2O_4$ calcined at 500°C	551
Co-precipitaion II, $CuFe_2O_4$ calcined at 750°C	645
Sol-gel, as-prepared $ZnFe_2O_4$	543
Sol-gel, as-prepared $MgFe_2O_4$	566

3.1.4. SEM and BET characterization

The SEM images of the different ferrite samples are depicted in Fig. 4. The first image (A) represents the as-prepared $CuFe_2O_4$ sample prepared by the sol-gel method. It shows porous, sponge-like particles. The formation of these pores might be due to the liberation of the entrapped gases during the combustion of the gel. The average pore diameter is determined by BET analysis, and it is equal to 15.8 nm, and the surface area is 25.18 m^2/g. The effect of calcination on the morphology of the sol-gel $CuFe_2O_4$ is illustrated in SEM images (A), (D) and (E). Comparing the images of the sol-gel as-prepared sample with that of the calcined samples clearly indicates that the number and size of the pores were decreased with increasing the calcination temperature up to 750°C.

Fig. 4(B) displays the SEM image of the as-prepared $CuFe_2O_4$ sample synthesized by co-precipitation method I. The image indicates that the particles are arranged as flakes. Moreover, agglomeration and elongation of the particles are

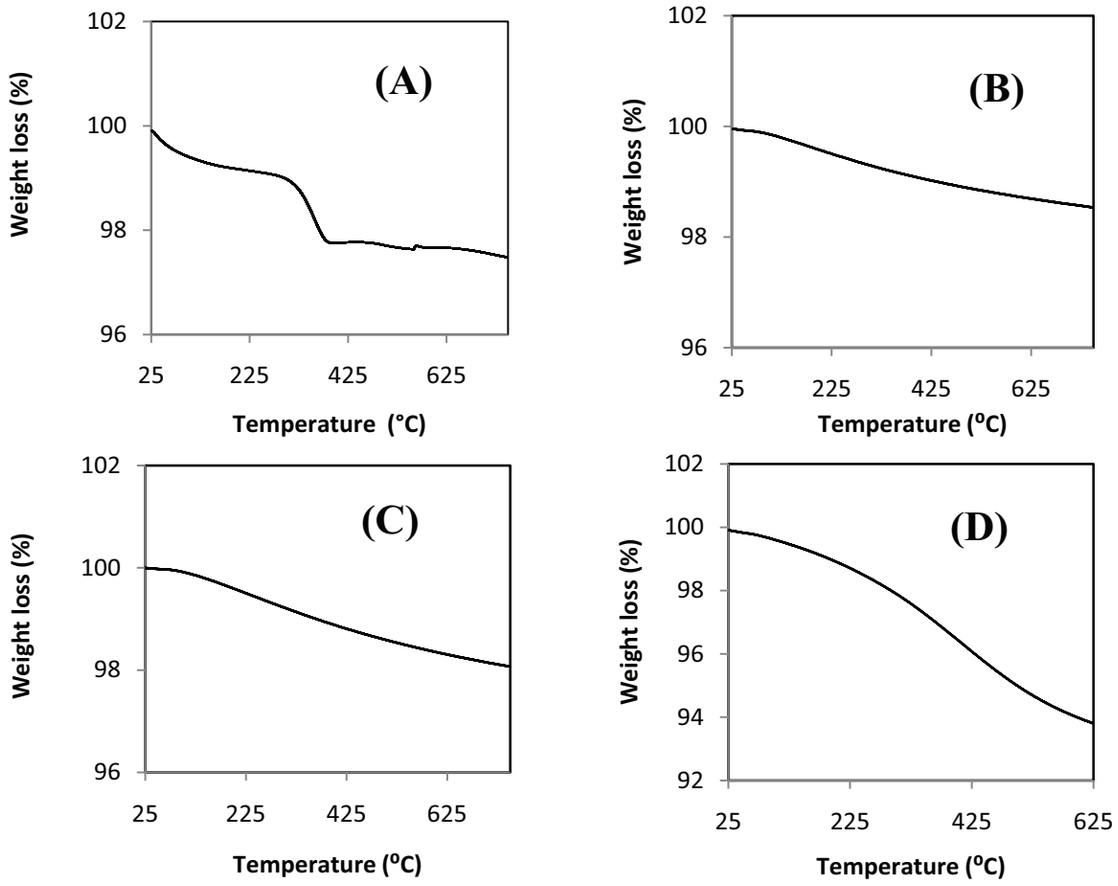

Fig. 3. TGA plots of different as-prepared ferrites: (A) $CuFe_2O_4$ prepared by sol-gel, (B) $ZnFe_2O_4$ prepared by sol-gel, (C) $MgFe_2O_4$ prepared by sol-gel, and (D) $CuFe_2O_4$ prepared by co-precipitation I.

observed. The BET analysis revealed that the average pore diameter is 2.8 nm, and the surface area is 41.7 m^2/g. On the other hand, a rugged surface of as-prepared $CuFe_2O_4$ synthesized by co-precipitation method II as shown in image (C).

Image (F) shows a porous, rough surface of the sol-gel, as-prepared $ZnFe_2O_4$. The surface area was measured using the BET analysis and found to be 80.9 m^2/g with pore size of 2.3 nm. Fig. 4(G) displays the SEM image of the sol-gel, as-prepared $MgFe_2O_4$, with a surface area of 79 m^2/g and pore size of 8.5 nm. Comparing images (A), (F), and (G) clearly indicates that the morphology of the different ferrites ($CuFe_2O_4$, $ZnFe_2O_4$, and $MgFe_2O_4$) prepared by the same method (sol-gel) varies with the chemical composition, in agreement with the literature [46].

3.1.5. TEM characterization

Fig. 5 presents the TEM images of different ferrite samples. The particle sizes of the as-prepared sol-gel and as-prepared co-precipitation derived $CuFe_2O_4$ samples were 25 and 7 nm, respectively. Such differences in the particle sizes reveal the effect of the preparation method on the size of the particles. Additionally, the TEM images illustrate that the size of the particles is affected by the chemical composition of the prepared ferrite, where the particle sizes of $CuFe_2O_4$ and $MgFe_2O_4$ are 25 and 80 nm, respectively. Moreover, the increase in particle size upon calcination was clearly noticed in the TEM analysis. The particle sizes of the different prepared ferrites are listed in the Table 2.

3.2. Phenol degradation reactions

3.2.1. Catalytic activity

To get an initial insight into the phenol degradation process, three experiments were carried out at room temperature as described in Section 2.3. An experiment examined the degradation reaction using the sol-gel, as-prepared $CuFe_2O_4$ catalyst only (without H_2O_2), while another experiment employed H_2O_2 only (without $CuFe_2O_4$ catalyst). The third experiment investigated the degradation reaction using both H_2O_2 and $CuFe_2O_4$. The results are displayed in Fig. 6 which clearly shows that the degradation of phenol occurred when both H_2O_2 and $CuFe_2O_4$ were used in the reaction mixture. In this degradation process, H_2O_2 acts as the source of hydroxyl radicals which are responsible for attacking and degrading phenol. The production of such radicals is induced by the $CuFe_2O_4$ catalyst. It is worth noting that no phenol removal

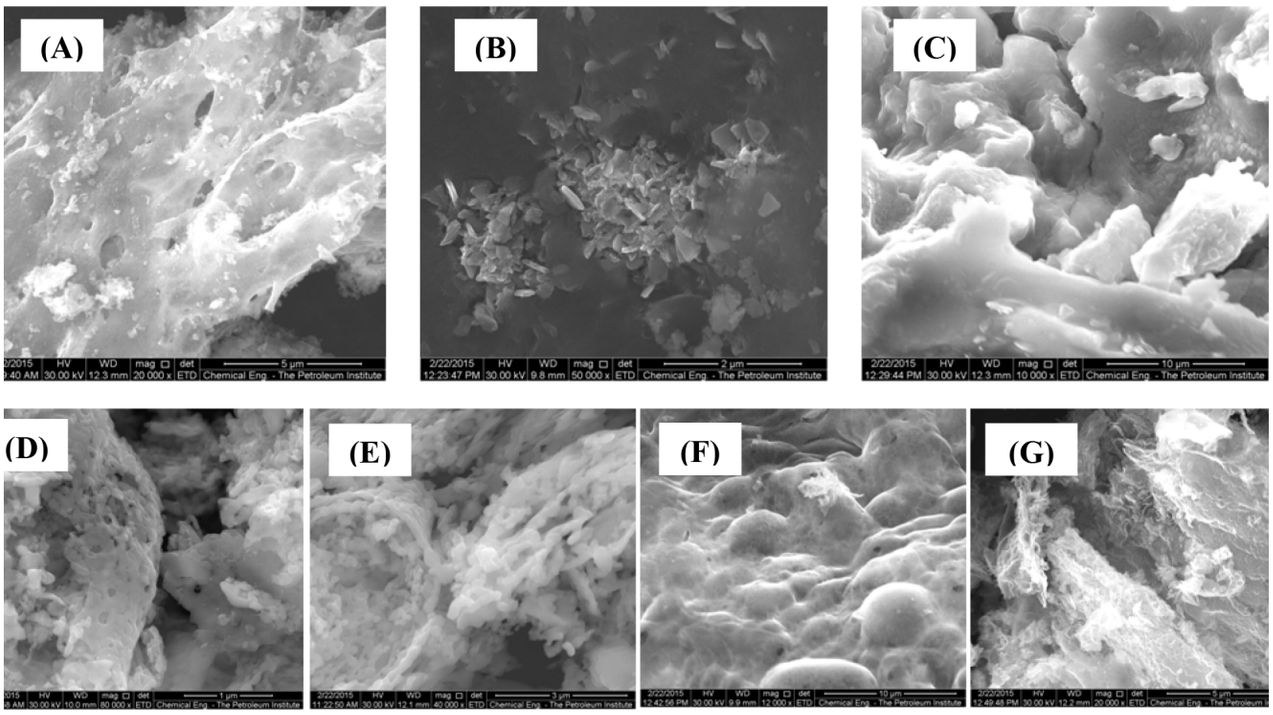

Fig. 4. SEM images of ferrite samples: (A) sol-gel, as-prepared $CuFe_2O_4$, (B) co-precipitation method I, as-prepared $CuFe_2O_4$, (C) co-precipitation method II, as-prepared $CuFe_2O_4$, (D) sol-gel, calcined at 500°C $CuFe_2O_4$, (E) sol-gel, calcined at 750°C $CuFe_2O_4$, (F) sol-gel, as-prepared $ZnFe_2O_4$, (G) sol-gel, as-prepared $MgFe_2O_4$.

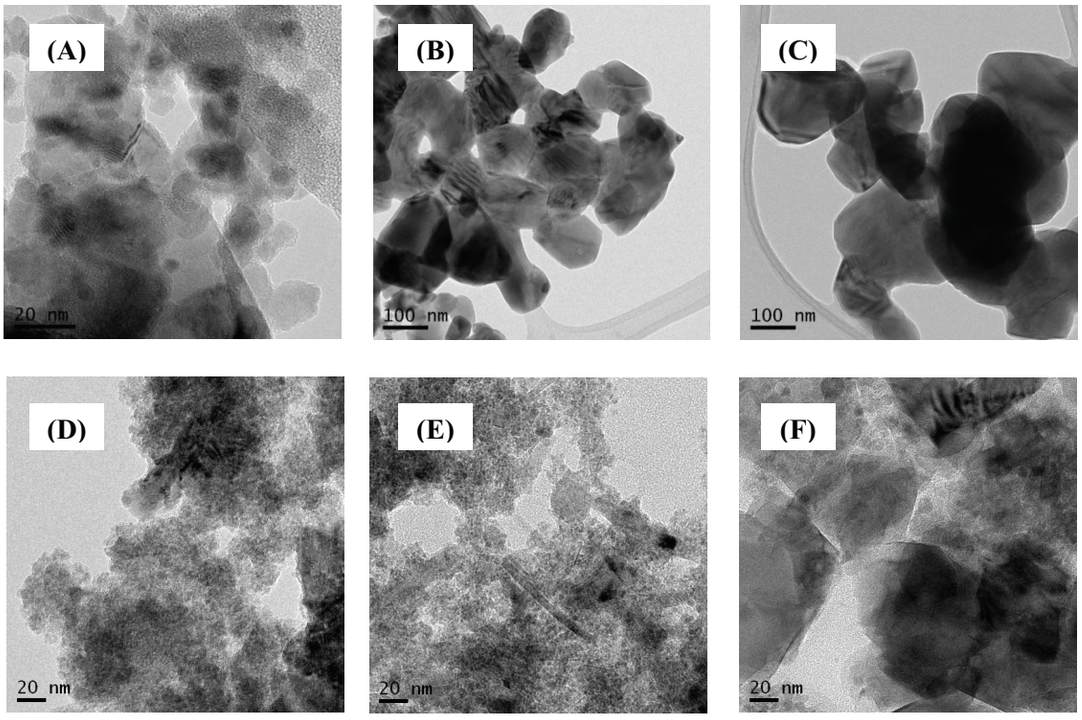

Fig. 5. TEM images of ferrite samples: (A) sol-gel, as-prepared $CuFe_2O_4$, (B) sol-gel, calcined at 500°C $CuFe_2O_4$, (C) sol-gel, calcined at 500°C $CuFe_2O_4$, (D) co-precipitation I, as-prepared $CuFe_2O_4$, (E) co-precipitation II,as-prepared $CuFe_2O_4$, and (F) sol-gel, as-prepared $MgFe_2O_4$.

Table 2
TEM particle size results of different ferrite samples

Sample name	Particle size range (nm)	Average particle size (nm)
Sol-gel, as-prepared $CuFe_2O_4$	10–35	25
Sol-gel $CuFe_2O_4$ calcined at 500°C	20–45	36.5
Sol-gel $CuFe_2O_4$ calcined at 750°C	25–45	36
Co-precipitaion I, as-prepared $CuFe_2O_4$	5–10	7.5
Co-precipitaion I, $CuFe_2O_4$ calcined at 500°C	5–15	7.5
Co-precipitaion I, $CuFe_2O_4$ calcined at 750°C	5–25	15
Co-precipitaion II, as-prepared $CuFe_2O_4$	5–8	6.5
Co-precipitaion II, $CuFe_2O_4$ calcined at 500°C	15–40	27.5
Co-precipitaion II, $CuFe_2O_4$ calcined at 750°C	20–45	32.5
Sol-gel, as-prepared $MgFe_2O_4$	10–150	80

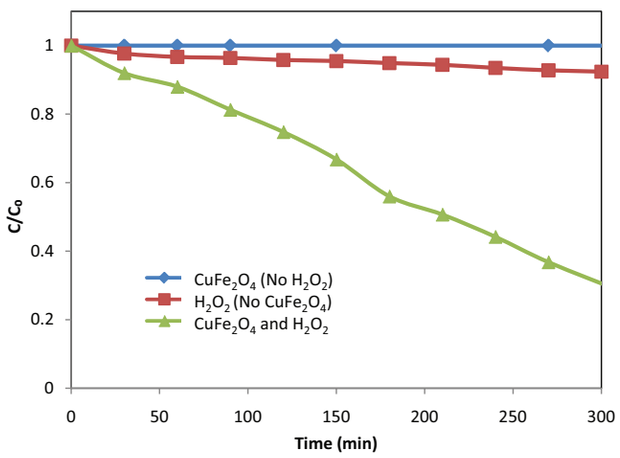

Fig. 6. Phenol removal in the presence of $CuFe_2O_4$ only, H_2O_2 only, or both $CuFe_2O_4$ and H_2O_2 (30 mg sol-gel, as-prepared $CuFe_2O_4$ catalyst, 1 M H_2O_2, 25°C, no pH adjustment, no UV or sunlight).

was observed when using $CuFe_2O_4$ only (without H_2O_2). This indicates that phenol does not directly react or adsorb onto the $CuFe_2O_4$ surface.

When using both H_2O_2 and $CuFe_2O_4$ in the reaction mixture, H_2O_2 can be activated on the $CuFe_2O_4$ surface and generates hydroxyl radicals which react with phenol in water. Such reaction can remove a hydrogen atom from the phenol ring and produce new radicals which may react again with H_2O_2 [47]:

$$HO^{\bullet} + phOH \rightarrow phO^{\bullet} + H_2O \quad (8)$$

$$phO^{\bullet} + H_2O_2 \rightarrow \text{oxidized products} \rightarrow CO_2 + H_2O \quad (9)$$

Accordingly, the degradation of phenol was mainly caused by the $CuFe_2O_4$ catalyst in the presence of H_2O_2. The rate of the phenol degradation reaction followed a first-order kinetics with respect to phenol concentration as shown in Fig. 7. According to Eq. (4), the reaction rate constant was found to be 3.3×10^{-3} min^{-1}.

3.2.2. Effect of different catalysts

The catalytic activity of the sol-gel, as-prepared $CuFe_2O_4$ towards phenol degradation was compared with the other sol-gel, as-prepared catalysts ($ZnFe_2O_4$ and $MgFe_2O_4$) and with the commercial TiO_2 catalyst. The results are shown in Fig. 8. The $CuFe_2O_4$ catalyst clearly exhibited the highest catalytic activity compared to the $ZnFe_2O_4$, $MgFe_2O_4$ and TiO_2 catalysts. About 65% of phenol was removed after 300 min when $CuFe_2O_4$ was used and the total removal of phenol was achieved after 8 h. However, after 300 min only 15% of phenol was removed when $MgFe_2O_4$ or TiO_2 were used, and only 2% of phenol was removed when $ZnFe_2O_4$ was used. Such variations in the catalytic activities among the used catalysts can be attributed to different electronic, chemical or structural properties of the different catalysts. Interest-

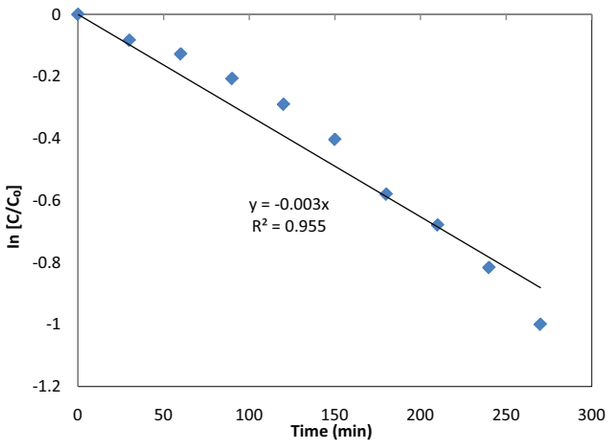

Fig. 7. First-order kinetics of phenol degradation in aqueous solution over sol-gel, as-prepared $CuFe_2O_4$ catalyst (30 mg catalyst, 1 M H_2O_2, 25°C).

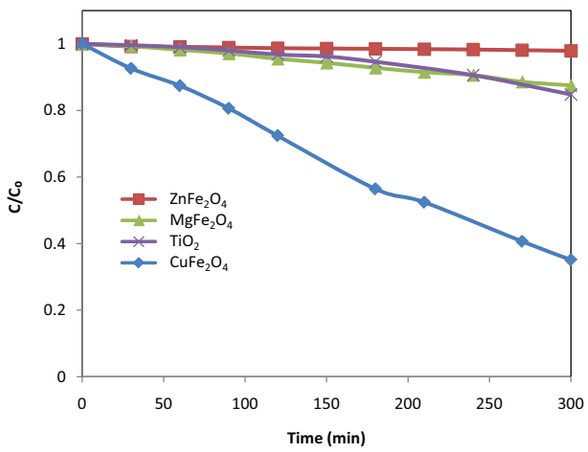

Fig. 8. Catalytic activities of sol-gel, as-prepared ferrites ($CuFe_2O_4$, $ZnFe_2O_4$ and $MgFe_2O_4$) and commercial TiO_2 (30 mg catalyst, 0.5 M H_2O_2, 25°C, no pH adjustment, no UV or sunlight).

ingly, the catalytic activity of the $CuFe_2O_4$ is significantly than that of TiO_2 which is considered as one of the most used catalysts in many industrial processes. All the degradation reactions followed a first-order kinetics as indicated in Table 3. The high catalytic activity of copper containing ferrites has been reported in the literature for reactions such as oxidation of organic dyes, decomposition of alcohols and benzoylation of aromatics [15,48–50]. The high activity of copper can be attributed to the presence of the redox pair Cu^+/Cu^{2+} at the catalyst surface where both can react with H_2O_2 producing hydroxyl radicals [15].

3.2.3. Effect of preparation method

The influence of the $CuFe_2O_4$ preparation method, sol-gel or co-precipitation, on the degradation of phenol was investigated. Fig. 9 demonstrates that the sol-gel as-prepared $CuFe_2O_4$ catalyst was the most active catalyst compared to the catalysts synthesized by co-precipitation methods I and II. After 5 h, for example, the phenol removal was about 65%, 45%, and 10%, for sol-gel, co-precipitation I, and co-precipitation II derived samples, respectively. The highest activity of sol-gel derived sample may be due to the high purity ferrite phase formed by this method, as confirmed by XRD measurements (Fig. 1(A)). Additionally, the different preparation methods lead to different surface morphologies and pore structures, as indicated by SEM images (Fig. 4). The sol-gel $CuFe_2O_4$ catalyst exhibited more pores, which may facilitate the generation of OH radicals that are responsible for phenol degradation. The reaction rate constants using the different $CuFe_2O_4$ catalysts are provided in Table 4.

Table 3
Reaction rate constants of phenol degradation using different catalysts

Type of catalyst	k (min^{-1})	R^2
$CuFe_2O_4$	2.7×10^{-3}	0.9825
$MgFe_2O_4$	5.0×10^{-4}	0.9935
TiO_2	2.0×10^{-4}	0.9326

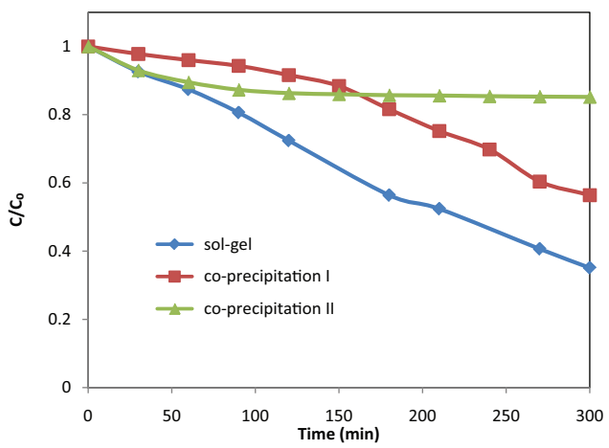

Fig. 9. Catalytic activities of as-prepared $CuFe_2O_4$ catalysts synthesized by sol-gel and co-precipitation I & II methods (30 mg catalyst, 0.5 M H_2O_2, 25°C, no pH adjustment, no UV or sunlight).

3.2.4. Effect of calcination temperature

Fig. 10 reveals that the catalytic efficiency of the sol-gel $CuFe_2O_4$ catalysts decreased as the calcination temperature increased. Thermal treatments at 500°C or 750°C of the sol-gel as-prepared $CuFe_2O_4$ resulted in larger particles with less pores, as shown in the SEM images. This may reduce the interactions between the catalyst and reactants, and consequently limiting the catalytic activity of the calcined $CuFe_2O_4$. The reaction rate coefficients are represented in Table 5.

3.2.5. Effect of catalyst loading

The influence of the sol-gel, as-prepared $CuFe_2O_4$ catalyst loading on the degradation of phenol is depicted in Fig. 11.

Table 4
Reaction rate constantsof phenol degradationusing $CuFe_2O_4$ catalysts prepared via different methods

Preparation method	k (min^{-1})	R^2
Sol-gel	2.7×10^{-3}	0.9825
Co-precipitation I	1.9×10^{-3}	0.9083

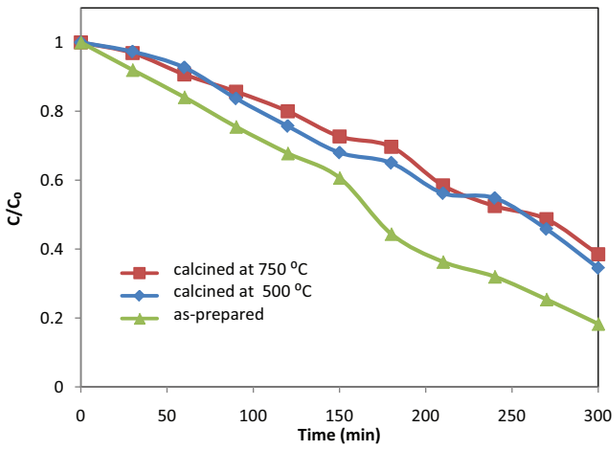

Fig. 10. Catalytic activities of $CuFe_2O_4$ catalysts prepared by sol-gel: as-prepared, calcined at 500°C, and calcined at 750°C (60 mg catalyst, 0.5 M H_2O_2, 25°C, no pH adjustment, no UV or sunlight).

Table 5
Reaction rate constants of phenol degradation using sol-gel $CuFe_2O_4$ calcined at different temperatures

Annealing temperature (°C)	k (min^{-1})	R^2
As-prepared	5.6×10^{-3}	0.9630
Calcined at 500°C	3.3×10^{-3}	0.9515
Calcined at 750°C	3.1×10^{-3}	0.9565

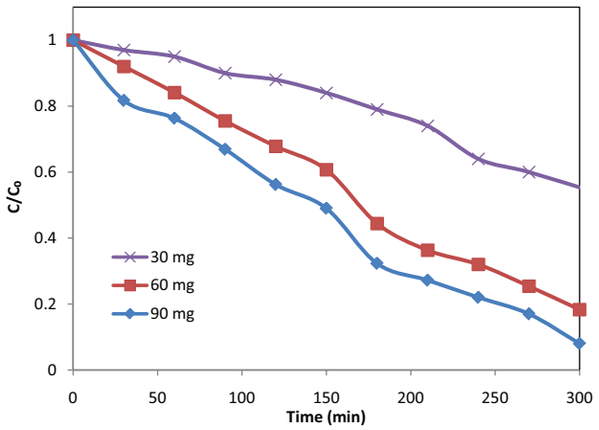

Fig. 11. The effect of sol-gel, as-prepared $CuFe_2O_4$ loading on the degradation of phenol (0.5 M H_2O_2, 25°C, no pH adjustment, no UV or sunlight).

Generally, a higher catalyst loading is expected to enhance the degradation of H_2O_2 and the generation of OH radicals, and consequently enhancing the degradation of phenol. However, increasing the catalyst loading and the amount of hydroxyl radicals may result in a scavenging effect in which H_2O_2 react with OH radicals instead of reacting with phenol [51]. The competition reaction between OH radicals and phenol will slow down the degradation process of phenol. As indicated by Fig. 11, using 90 mg of $CuFe_2O_4$ slightly enhanced the degradation of phenol as compared to the reaction with 60 mg of $CuFe_2O_4$. In both cases, the removal percentage of phenol after 24 h was 100%. Another explanation can be the agglomeration of the catalyst particles as the loading increases and consequently reducing the available active sites on the catalyst surface [52]. The reactions followed a first order kinetics, and the rate constants are presented in Table 6.

3.2.6. Effect of reaction temperature

The phenol degradation efficiency by the sol-gel, as-prepared $CuFe_2O_4$ catalyst at different reaction temperatures is presented in Fig. 12. As can be observed, the degradation of phenol was increased by increasing the reaction temperature. Phenol was completely removed after 30 min at 50°C and after 90 min at 40°C. While for the reaction conducted at room temperature, complete removal phenol from the solution was observed after 24 h. This can be attributed to the fact that at elevated temperatures more vigorous collisions between molecules occur, and therefore a faster degradation process is expected [53]. However, raising the temperature up to a certain level might deplete the removal of phenol due to the increment in the decomposition rate of H_2O_2 to O_2 and H_2O [51,54].

Table 6
Reaction rate constants of phenol degradation using different loadings of the sol-gel, as-prepared $CuFe_2O_4$ catalyst

Catalyst loading (mg)	k (min^{-1})	R^2
30	2.7×10^{-3}	0.9825
60	5.6×10^{-3}	0.9630
90	7.6×10^{-3}	0.9382

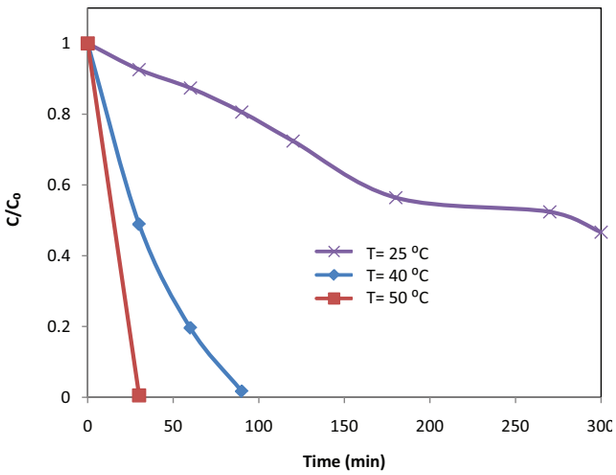

Fig. 12. Effect of temperature on the degradation of phenol using sol-gel, as-prepared $CuFe_2O_4$ (30 mg catalyst, 0.5 M H_2O_2, no pH adjustment, no UV or sunlight).

The reaction rate constants (k) were determined at 298 and 313 k and found to be 0.0027 and 0.0272 min^{-1}, respectively. The activation energy E_a was then calculated according to Eq. (6) and found to be 120 kJ/mol.

3.2.7. Effect of initial pH

A sequence of pH adjustments of phenol solutions was conducted using 0.1 M HCl or 0.1 M NaOH to study the influence of pH on the phenol degradation. The pH is expected to affect the stability of hydrogen peroxide, the stability of the catalyst, and the phenol degradation mechanism [55]. Fig. 13 shows the effect of the initial pH of the solution on the degradation of phenol. Obviously, more phenol removal was achieved under acidic conditions, in

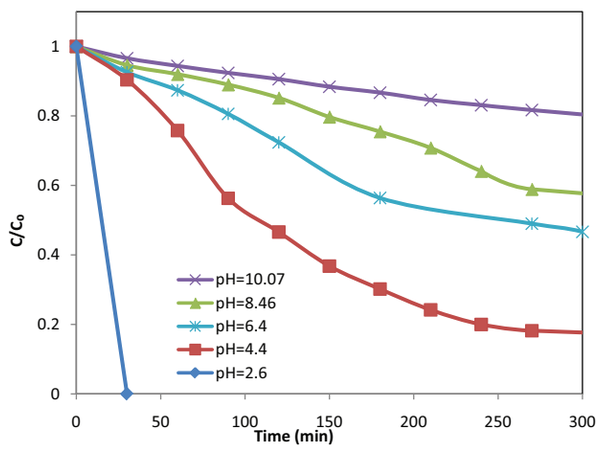

Fig. 13. Effect of initial pH on the degradation of phenol using sol-gel, as-prepared $CuFe_2O_4$ (30 mg catalyst, 0.5 M H_2O_2, 25°C, no UV or sunlight).

agreement with the literature [56,57]. At a pH of 2.6, phenol was completely removed within 30 min, but more time was required to remove phenol at high pH values. However, extremely acidic pH solutions can cause the metals to leach out from the catalyst to the solution, and consequently acting as a homogenous catalyst. Under alkaline conditions, H_2O_2 can be decomposed into O_2 and H_2O instead of free hydroxyl radicals which reduce the degradation of phenol [1]. The reactions follow first-order kinetics as can be deduced from Table 7.

3.2.8. Effect of H_2O_2 concentration and addition mode

Phenol degradation was investigated at different initial concentrations of H_2O_2. Fig. 14 shows that reactions at higher H_2O_2 concentrations promote a faster phenol removal. A higher H_2O_2 concentration may result in a higher production of hydroxyl radicals which in turn facilitates the degradation of phenol [56]. However, further increase of H_2O_2 concentration may induce other reactions which negatively influence the phenol removal efficiency. An excess amount of H_2O_2 may increase the chance for OH radicals to react with H_2O_2 and produce the less active HO_2 radicals in a process called self-quenching [52,58]. A complete removal of phenol for each of the tested H_2O_2 concentrations was achieved after 24 h at room temperature. The reaction rate constants are displayed in Table 8.

Table 7
Reaction rate constants of phenol degradation under various initial pH values

pH	% Phenol remained after 300 min	k (min^{-1})	R^2
4.4	22%	6.8×10^{-3}	0.9882
6.4	43%	2.7×10^{-3}	0.9825
8.46	60%	1.9×10^{-3}	0.9690
10.07	83%	7.0×10^{-4}	0.9954

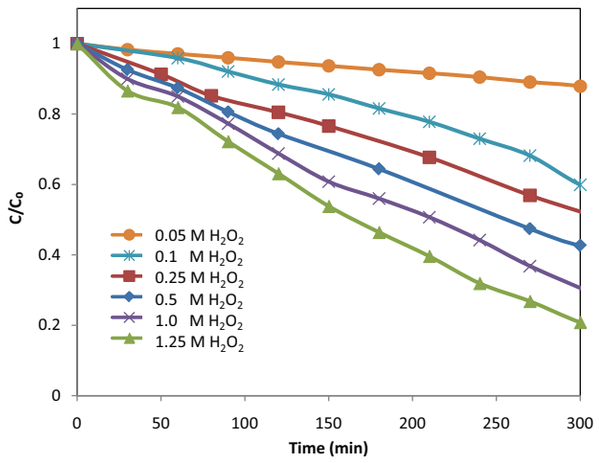

Fig. 14. Effect of H_2O_2 concentration on the degradation of phenol using sol-gel, as-prepared $CuFe_2O_4$ (30 mg catalyst, 25°C, no pH adjustment, no UV or sunlight).

Table 8
Reaction rate constants of phenol degradation under several H_2O_2 concentrations

H_2O_2 concentration (M)	k (min^{-1})	R^2
1.25	5.1×10^{-3}	0.9818
1	3.3×10^{-3}	0.9558
0.5	2.7×10^{-3}	0.9825
0.25	2.0×10^{-3}	0.9886
0.1	1.6×10^{-3}	0.9413
0.05	4.0×10^{-4}	0.9982

Two addition modes of H_2O_2 to the reaction mixture were examined for the degradation of phenol. One mode was achieved by adding 5 mL of H_2O_2 continuously to the reaction mixture with a feeding rate equal to 0.14 mL/min using a peristaltic pump. The second mode was carried out by entirely adding 5 mL of H_2O_2 as a single-shot at the beginning of the reaction. Fig. 15(A) indicates that the removal efficiency is higher for the continuous addition of H_2O_2 compare to the single-shot addition. The percent phenol removed in both reactions after 210 min is around 45% for the single-shot addition mode and 59% for the continuous addition mode. In the single-shot addition mode, starting with a high concentration of H_2O_2 at the beginning of the reaction may promoted the self-quenching effect of OH radicals giving lower chance for phenol to be attacked by the OH radicals. In contrast, the continuous addition of H_2O_2 in small amounts will decrease its scavenging effect and in this case the produced OH radicals will have higher chance to attack and degrade phenol.

In order to test the influence of the feeding rate of H_2O_2 on the degradation process, two different feeding rates of 0.14 and 0.07 mL/min were examined in the continuous mode under the same reaction conditions. The removal of phenol at both flow rates after 250 min was around 14% and 16%, respectively, as revealed in Fig. 15(B). Apparently, changing the feeding rate doesn't considerably affect the degradation efficiency of phenol. Table 9 represents the rate constant values of the reactions of different addition modes of H_2O_2 and different flow rates.

3.2.9. Effect of UV radiation and stirring

To further study the degradation process of phenol, the effect of UV radiation was investigated. Two reaction mixtures were subjected to UV radiation (using a UV lamp, UVGL-58 Handheld) at a wavelength of 254 nm. One reaction mixture was stirred and the other one was kept without stirring, and the results are presented in Fig. 16. For comparison purposes, two additional reactions (with and without stirring) were carried out without being subjected to UV radiation, and the results are displayed in Fig. 17. Comparing Figs. 16 and 17 clearly indicates that the degradation of phenol is enhanced under UV radiation. After 300 min, the phenol removal without UV radiation was only 50% with stirring and 77% without stirring conditions, whereas phenol removal under UV radiation reached 85% with stirring and 100% without stirring conditions.

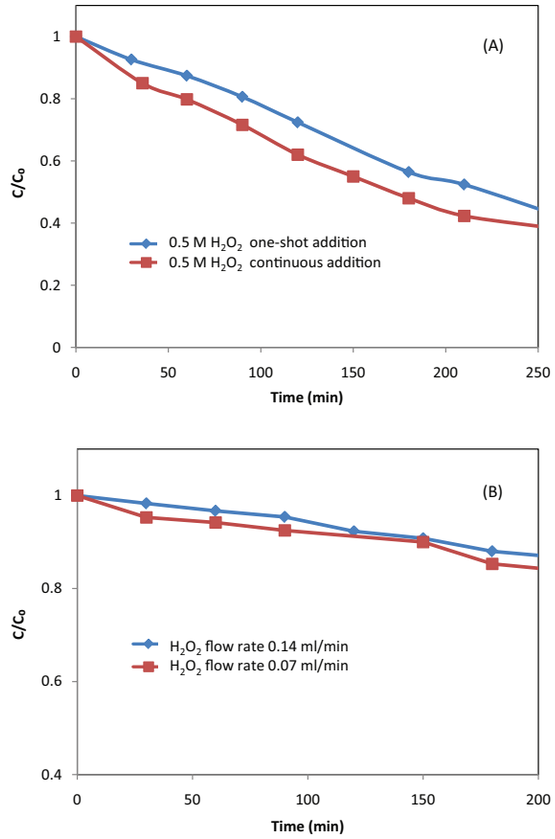

Fig. 15. Removal of phenol using sol-gel, as-prepared $CuFe_2O_4$: (A) effect of H_2O_2 addition mode and (B) effect of H_2O_2 addition flow rate (30 mg catalyst, 25°C, no pH adjustment, no UV or sunlight).

Table 9
Reaction rate constants of phenol degradation under different H_2O_2 addition modes and flow rates

	k (min^{-1})	R^2
Addition mode		
Single-shot	2.7×10^{-3}	0.9825
Continuous	3.9×10^{-3}	0.9942
Flow rate (mL/min)		
0.14	3.9×10^{-3}	0.9942
0.07	3.2×10^{-3}	0.9626

Fig. 17 represents the effect of stirring on the degradation reaction of phenol without UV radiation. Interestingly, the results suggest that the phenol degradation with no stirring is higher than the one carried out with stirring (at 300 rpm). This may be attributed to lower interactions of H_2O_2 with the catalyst surface under stirring conditions which leads to a lower decomposition of H_2O_2 into OH radicals.

Under UV radiation (Fig. 16), more phenol degradation was achieved with no stirring condition compared to the stirring condition. The stirring of the reaction mixture made it more turbid which may reduce the penetration of the UV radiation into the reaction mixture. As a result, less OH radicals were generated and less degradation of phenol was obtained.

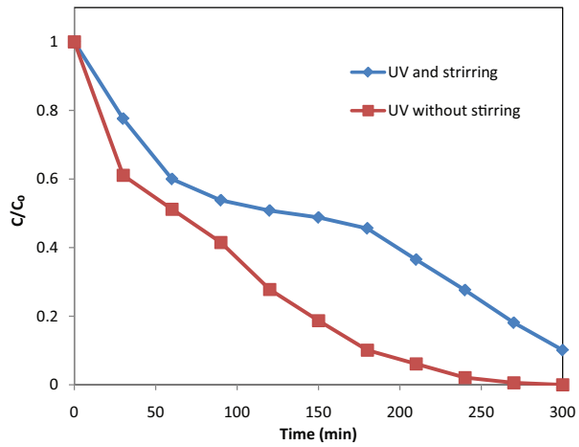

Fig. 16. Effect of UV radiation on the degradation of phenol under different stirring conditions (30 mg catalyst, 25°C, 0.5 M H_2O_2, no pH adjustment).

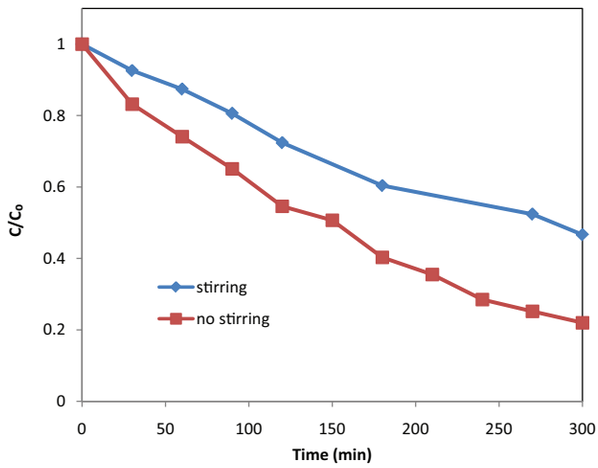

Fig. 17. Effect of stirring on the degradation of phenol (30 mg catalyst, 0.5 H_2O_2, 25°C, no pH adjustment, no UV or sunlight).

As a photocatalyst, it is expected that UV radiation enhances the activity of $CuFe_2O_4$ towards the decomposition of H_2O_2 and phenol (a photo-Fenton process). This can be simplified as the photo reduction of ferric ions (Fe^{3+}) to ferrous ions (Fe^{2+}) as in the following equation [52]:

$$Fe(OH)^{2+} + hvFe^{2} \rightarrow HO \quad (10)$$

These ferrous ions (Fe^{2+}) will consequently react with H_2O_2 and generate OH radicals according to Eq. (1). Moreover, when $CuFe_2O_4$ interact with UV radiation, the electrons in the valence band will be excited into the conduction band producing photo generated holes. The produced electron-hole pairs enable the oxidation and reduction reactions that degrade phenol molecules. In addition, water molecules react with the photo generated holes and generate OH radicals which can also contribute to the degradation of phenol [12]. In addition, the direct photolysis

of H_2O_2 by UV irradiation can contribute to the formation of OH radicals, and hence to the degradation of phenol according to the following reaction [59]:

$$H_2O_2 + Hv2 \rightarrow HO \quad (11)$$

3.2.10. Effect of sunlight

To study the effect of sunlight on the catalytic activity of sol-gel as-prepared $CuFe_2O_4$, a mixture of 100 ml of phenol and 30 mg of the catalyst was kept under sunlight. One drop of H_2O_2 was added to the reaction mixture every 15 min. For comparison, the same experiment was carried out under the same conditions by using the other prepared sol-gel ferrite catalysts ($ZnFe_2O_4$ and $MgFe_2O_4$), and the commercial TiO_2. As illustrated in Fig. 18, the activity of the catalysts towards phenol degradation found to be: $ZnFe_2O_4$ < $MgFe_2O_4$ < TiO_2 < $CuFe_2O_4$.

Fig. 19 compares the photo degradation of phenol under UV radiation and under sunlight using the sol-gel, as-prepared $CuFe_2O_4$. The figure reveals that after 160 min the removal of phenol reached 100% under sunlight compared to only 55% under UV radiation. The higher performance of $CuFe_2O_4$ under sunlight can be related to wider spectrum and variety of wavelengths provided by sunlight. For example, sunlight consists of 46% visible light, 49% infrared radiation and only 5% UV radiation [12]. Economically, this is important since sunlight is readily available and costless in contrast to the expensive UV radiation.

Titanium dioxide was further tested for phenol degradation under sunlight and without sunlight. Fig. 20 clearly shows that the catalytic activity of $TiO_2$was high only under sunlight. Interestingly, the sol-gel as-prepared $CuFe_2O_4$ catalyst was active with or without radiation, unlike TiO_2 which needs sunlight to be an active catalyst.

3.3. Regeneration of copper ferrite catalyst

The sol-gel as-prepared $CuFe_2O_4$ catalyst was recovered after the reaction by filtration and then dried over-

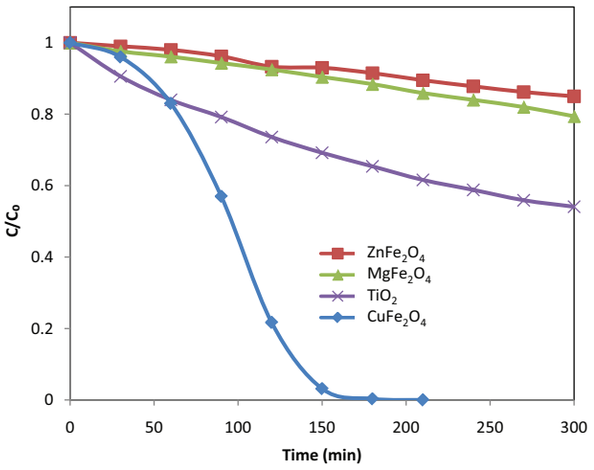

Fig. 18. Effect of the sunlight on the degradation of phenol using different catalysts (30 mg catalyst, one drop H_2O_2 every 15 min, no pH adjustment).

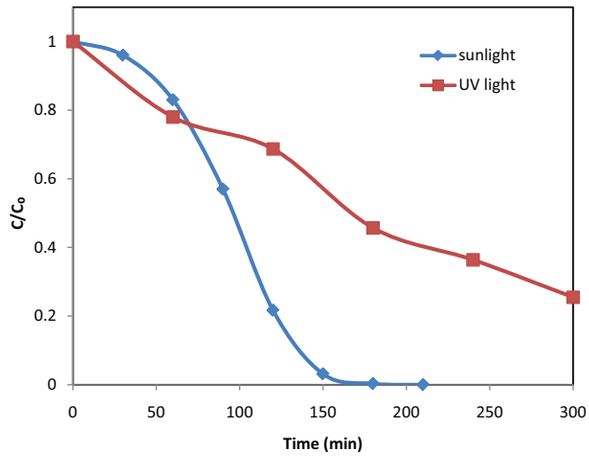

Fig. 19. Effect of the sunlight or UV radiation on the degradation of phenol using sol-gel, as-prepared $CuFe_2O_4$ (30 mg catalyst, one drop H_2O_2 every 15 min, no pH adjustment).

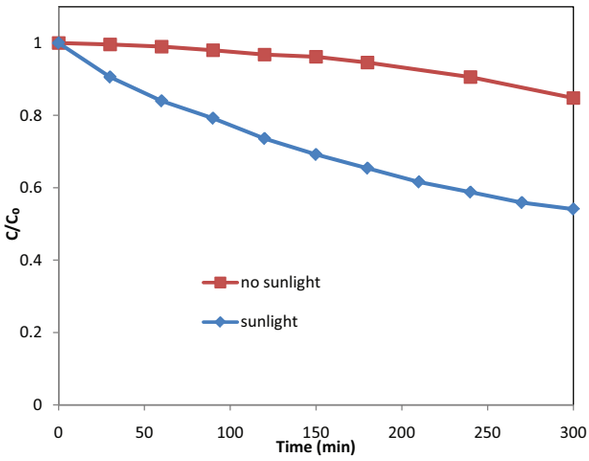

Fig. 20. Effect of sunlight on the activity of TiO_2 toward phenol degradation (30 mg catalyst, one drop H_2O_2 every 15 min under sunlight or 0.5 M H_2O_2 if no sunlight, no pH adjustment).

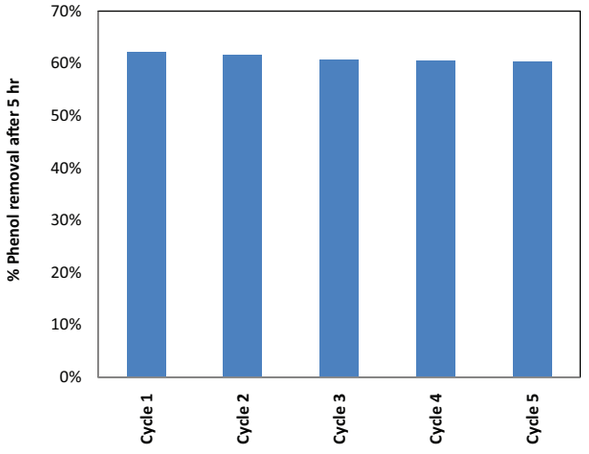

Fig. 21. Effect of regeneration and repeated cycles of the sol-gel $CuFe_2O_4$ catalyst on removal of phenol (30 mg catalyst, 0.5 H_2O_2, 25°C, no pH adjustment, no UV or sunlight).

night in an oven at 130°C in order to be used in the next reaction. The $CuFe_2O_4$ catalyst was regenerated and reused five cycles without significant loss in its catalytic activity as shown in Fig. 21. This is a major requirement in industrial applications since the catalyst can be easily regenerated and successfully reused in successive reactions. Complete phenol removal was achieved in all cycles after 24 h at room temperature using the regenerated $CuFe_2O_4$.

4. Conclusions

Copper ferrites ($CuFe_2O_4$) nanoparticles were successfully prepared by sol-gel auto combustion and co-precipitation methods. The catalytic properties of the $CuFe_2O_4$ nanoparticles were investigated in the Fenton reaction for the degradation of phenol in aqueous solutions. $CuFe_2O_4$ catalysts synthesized via the sol-gel route were characterized by higher porosity, purity, crystallinity and catalytic activity compared to the $CuFe_2O_4$ catalysts obtained by the co-precipitation method. $CuFe_2O_4$ catalysts were found to lose their catalytic activity towards phenol degradation when calcined at elevated temperatures. The $CuFe_2O_4$ catalyst showed the highest activity towards phenol degradation among other catalysts, with the following order: $CuFe_2O_4 > TiO_2 > MgFe_2O_4 > ZnFe_2O_4$. The phenol degradation process using sol-gel, as-prepared $CuFe_2O_4$ catalysts was investigated under different experimental condition such as the solution pH, reaction temperature, H_2O_2 concentration, catalyst loading, H_2O_2 addition mode, stirring, and the presence of UV or sunlight radiations. The degradation rate was enhanced by increasing the H_2O_2 concentrations or increasing the $CuFe_2O_4$ catalyst loadings. Moreover, complete removal of phenol and its intermediate products was achieved at high reaction temperatures, acidic pH, or presence of UV or sunlight radiation. The $CuFe_2O_4$ catalyst was successfully regenerated and reused effectively up to five cycles without significant loss in its catalytic activity. The $CuFe_2O_4$ catalyst can be a potential catalyst in treating industrial wastewater.

Acknowledgement

The authors are grateful to the Research Office at The Petroleum Institute, Abu Dhabi, for funding project [# 14513].

References

[1] P. Wang, X. Bian, Y. Li, Catalytic oxidation of phenol in wastewater — a new application of the amorphous $Fe_{78}Si_9B_{13}$ alloy, Chin. Sci. Bull., 57 (2012) 33–40.
[2] M. Choquette-Labbé, W. Shewa, J. Lalman, S. Shanmugam, Photocatalytic degradation of phenol and phenol derivatives using a nano-TiO_2 catalyst: integrating quantitative and qualitative factors using response surface methodology, Water, 6 (2014) 1785.
[3] L.F. Liotta, M. Gruttadauria, G. Di Carlo, G. Perrini, V. Librando, Heterogeneous catalytic degradation of phenolic substrates: catalysts activity, J. Hazard. Mater., 162 (2009) 588–606.
[4] A.S. Whiteley, M.J. Bailey, Bacterial community structure and physiological state within an industrial phenol bioremediation system, Appl. Environ. Microbiol., 66 (2000) 2400–2407.
[5] Y.-H. Shen, Removal of phenol from water by adsorption–flocculation using organobentonite, Water Res., 36 (2002) 1107–1114.
[6] F.A. Banat, B. Al-Bashir, S. Al-Asheh, O. Hayajneh, Adsorption of phenol by bentonite, Environ. Pollut., 107 (2000) 391–398.
[7] R. Mukherjee, S. De, Adsorptive removal of phenolic compounds using cellulose acetate phthalate–alumina nanoparticle mixed matrix membrane, J. Hazard. Mater., 265 (2014) 8–19.
[8] Y.B. Feng, L. Hong, A.L. Liu, W.D. Chen, G.W. Li, W. Chen, X.H. Xia, High-efficiency catalytic degradation of phenol based on the peroxidase-like activity of cupric oxide nanoparticles, Int. J. Environ. Sci. Technol., 12 (2013) 653–660.
[9] U. Bali, E.Ç. Çatalkaya, F. Şengül, Photochemical degradation and mineralization of phenol: a comparative study, J. Environ. Sci. Health, Pt. A, 38 (2003) 2259–2275.
[10] Y. Tao, Z.L. Cheng, K.E. Ting, X.J. Yin, Photocatalytic degradation of phenol using a nanocatalyst: the mechanism and kinetics, J. Catalysts, 2013 (2013) 6.
[11] M. Pera-Titus, V. García-Molina, M.A. Baños, J. Giménez, S. Esplugas, Degradation of chlorophenols by means of advanced oxidation processes: a general review, Appl. Catal. B, 47 (2004) 219–256.
[12] E. Casbeer, V.K. Sharma, X.-Z. Li, Synthesis and photocatalytic activity of ferrites under visible light: a review, Sep. Purif. Technol., 87 (2012) 1–14.
[13] P.V. Nidheesh, Heterogeneous Fenton catalysts for the abatement of organic pollutants from aqueous solution: a review, RSC Adv., 5 (2015) 40552–40577.
[14] S.-Q. Liu, L.-R. Feng, N. Xu, Z.-G. Chen, X.-M. Wang, Magnetic nickel ferrite as a heterogeneous photo-Fenton catalyst for the degradation of rhodamine B in the presence of oxalic acid, Chem. Eng. J., 203 (2012) 432–439.
[15] A.S. Albuquerque, M.V.C. Tolentino, J.D. Ardisson, F.C.C. Moura, R. de Mendonça, W.A.A. Macedo, Nanostructured ferrites: structural analysis and catalytic activity, Ceram. Int., 38 (2012) 2225–2231.
[16] Q. Chen, Z.J. Zhang, Size-dependent superparamagnetic properties of $MgFe_2O_4$ spinel ferrite nanocrystallites, Appl. Phys. Lett., 73 (1998) 3156–3158.
[17] P. Vaqueiro, M. Arturo Lopez-quintela, Synthesis of yttrium aluminium garnet by the citrate gel process, J. Mater. Chem., 8 (1998) 161–163.
[18] C.W. Lim, I.S. Lee, Magnetically recyclable nanocatalyst systems for the organic reactions, Nano Today, 5 (2010) 412–434.
[19] S.D. Sartale, C.D. Lokhande, M. Muller, Electrochemical synthesis of nanocrystalline $CuFe_2O_4$ thin films from non-aqueous (ethylene glycol) medium, Mater. Chem. Phys., 80 (2003) 120–128.
[20] K.-S. Kang, C.-H. Kim, W.-C. Cho, K.-K. Bae, S.-W. Woo, C.-S. Park, Reduction characteristics of $CuFe_2O_4$ and Fe_3O_4 by methane; $CuFe_2O_4$ as an oxidant for two-step thermochemical methane reforming, Int. J. Hydrogen Energy, 33 (2008) 4560–4568.
[21] N. Nasrallah, M. Kebir, Z. Koudri, M. Trari, Photocatalytic reduction of Cr(VI) on the novel hetero-system $CuFe_2O_4$/CdS, J. Hazard. Mater., 185 (2011) 1398–1404.
[22] M.M. Rashad, R.M. Mohamed, M.A. Ibrahim, L.F.M. Ismail, E.A. Abdel-Aal, Magnetic and catalytic properties of cubic copper ferrite nanopowders synthesized from secondary resources, Adv. Powder Technol., 23 (2012) 315–323.
[23] J.-C. Lou, C.-K. Chang, Catalytic oxidation of CO over a catalyst produced in the ferrite process, Environ. Eng. Sci., 23 (2006) 1024–1032.
[24] Y.L.N. Murthy, B.S. Diwakar, B. Govindh, K. Nagalakshmi, I.V.K. Viswanath, R. Singh, Nano copper ferrite: a reusable catalyst for the synthesis of β, γ-unsaturated ketones, J. Chem. Sci., 124 (2012) 639–645.
[25] A. Gharib, N. Noroozi Pesyan, L. Vojdani Fard, M. Roshani, Catalytic synthesis of a-aminonitriles using nano copper ferrite under green conditions, Org. Chem. Int., 2014 (2014) 8.
[26] S. Rahman, K. Nadeem, M. Anis-ur-Rehman, M. Mumtaz, S. Naeem, I. Letofsky-Papst, Structural and magnetic properties of ZnMg-ferrite nanoparticles prepared using the co-precipitation method, Ceram. Int., 39 (2013) 5235–5239.
[27] B.K. Chatterjee, K. Bhattacharjee, A. Dey, C.K. Ghosh, K.K. Chattopadhyay, Influence of spherical assembly of copper ferrite nanoparticles on magnetic properties: orientation of magnetic easy axis, Dalton Trans., 43 (2014) 7930–7944.

[28] R. Köferstein, T. Walther, D. Hesse, S.G. Ebbinghaus, Crystallite-growth, phase transition, magnetic properties, and sintering behaviour of nano-$CuFe_2O_4$ powders prepared by a combustion-like process, J. Solid State Chem., 213 (2014) 57–64.
[29] J. Wu, X. Wang, H. Kang, J. Zhang, C. Yang, $CuFe_2O_4$ As heterogeneous catalyst in degradation of p-nitrophenol with photoelectron-fenton-like process, Int. J. Environ. Stud., 71 (2014) 534–545.
[30] J. Zheng, Z. Lin, W. Liu, L. Wang, S. Zhao, H. Yang, L. Zhang, One-pot synthesis of $CuFe_2O_4$ magnetic nanocrystal clusters for highly specific separation of histidine-rich proteins, J. Mater. Chem. B, 2 (2014) 6207–6214.
[31] R. Koferstein, T. Walther, D. Hesse, S.G. Ebbinghaus, Preparation and characterization of nanosized magnesium ferrite powders by a starch-gel process and corresponding ceramics, J. Mater. Sci., 48 (2013) 6509–6518.
[32] A. Loganathan, K. Kumar, Effects on structural, optical, and magnetic properties of pure and Sr-substituted $MgFe_2O_4$ nanoparticles at different calcination temperatures, Appl. Nanosci., 6 (2016) 629–639.
[33] Z. Jia, D. Ren, Y. Liang, R. Zhu, A new strategy for the preparation of porous zinc ferrite nanorods with subsequently light-driven photocatalytic activity, Mater. Lett., 65 (2011) 3116–3119.
[34] T. Tsoncheva, E. Manova, N. Velinov, D. Paneva, M. Popova, B. Kunev, K. Tenchev, I. Mitov, Thermally synthesized nanosized copper ferrites as catalysts for environment protection, Catal. Commun., 12 (2010) 105–109.
[35] J.E. Tasca, C.E. Quincoces, A. Lavat, A.M. Alvarez, M.G. González, Preparation and characterization of $CuFe_2O_4$ bulk catalysts, Ceram. Int., 37 (2011) 803–812.
[36] Z. Zhu, F. Liu, H. Zhang, J. Zhang, L. Han, Photocatalytic degradation of 4-chlorophenol over Ag/MFe_2O_4 (M = Co, Zn, Cu, and Ni) prepared by a modified chemical co-precipitation method: a comparative study, RSC Adv., 5 (2015) 55499–55512.
[37] N.M. Deraz, Production and characterization of pure and doped copper ferrite nanoparticles, J. Anal. Appl. Pyrolysis, 82 (2008) 212–222.
[38] M. Farid, I. Ahmad, S. Aman, M. Kanwal, G. Murtaza, I. Alia, M. Ishfaq, SEM, FTIR and dielectric properties of cobalt substituted spinel ferrites, J. Ovon Res., 11 (2015) 1–10.
[39] A. Pradeep, G. Chandrasekaran, FTIR study of Ni, Cu and Zn substituted nano-particles of $MgFe_2O_4$, Mater. Lett., 60 (2006) 371–374.
[40] J.D. Kisan Zipare, Sushil Bandgar, Vikas Mathe, Guruling Shahane, Superparamagnetic manganese ferrite nanoparticles: synthesis and magnetic properties, J. Nanosci. Nanoeng., 1 (2015) 178–182.
[41] N.M. Mahmoodi, Zinc ferrite nanoparticle as a magnetic catalyst: synthesis and dye degradation, Mater. Res. Bull., 48 (2013) 4255–4260.
[42] H. Jiao, G. Jiao, J. Wang, Preparation and magnetic properties of $CuFe_2O_4$ nanoparticles, Synth. React. Inorg. Me., 43 (2013) 131–134.
[43] Y. Ding, Y. Yang, H. Shao, Synthesis and characterization of nanostructured $CuFe_2O_4$ anode material for lithium ion battery, Solid State Ionics, 217 (2012) 27–33.
[44] A.R. Tehrani-Bagha, M. Gharagozlou, F. Emami, Catalytic wet peroxide oxidation of a reactive dye by magnetic copper ferrite nanoparticles, J. Environ. Chem. Eng., 4 (2016) 1530–1536.
[45] Amarjeet, V. Kumar, Synthesis, thermal and FTIR study of Zn-Fe nano ferrites, Int. J. Lat. Res. Sci. Technol., 3 (2014) 61–63.
[46] N. Rezlescu, E. Rezlescu, F. Tudorache, P.D. Popa, Gas sensing properties of porous Cu-, Cd- and Zn- ferrites, Rom. Rep. Phys., 61 (2009) 223–234.
[47] G.V. Buxton, C.L. Greenstock, W.P. Helman, W.P. Ross, Critical review of rate constants for reactions of hydrated electrons, hydrogen atoms and hydroxyl radicals in aqueous solution, J. Phys. Chem. Ref. Data, 17 (1988) 513–886.
[48] P. Baldrian, V. Merhautova, J. Gabriel, F. Nerud, P. Stopka, M. Hruby, M.J. Benes, Decolorization of synthetic dyes by hydrogen peroxide with heterogeneous catalysis by mixed iron oxides, Appl. Catal., B, 66 (2006) 258–264.
[49] C. Ramankutty, S. Sugunan, B. Thomas, Study of cyclohexanol decomposition reaction over the ferrospinels, A_{1-x} Cu_x Fe_2O_4 (A= Ni or Co and x= 0, 0.3, 0.5, 0.7 and 1), prepared by 'soft'chemical methods, J. Mol. Catal. A, 187 (2002) 105–117.
[50] C.G. Ramankutty, S. Sugunan, Surface properties and catalytic activity of ferrospinels of nickel, cobalt and copper, prepared by soft chemical methods, Appl. Catal., A, 218 (2001) 39–51.
[51] Y. Zhao, G. He, W. Dai, H. Chen, High catalytic activity in the phenol hydroxylation of magnetically separable $CuFe_2O_4$–reduced graphene oxide, Ind. Eng. Chem. Res., 53 (2014) 12566–12574.
[52] L. Roshanfekr Rad, B. Farshi Ghazani, M. Irani, M. Sadegh Sayyafan, I. Haririan, Comparison study of phenol degradation using cobalt ferrite nanoparticles synthesized by hydrothermal and microwave methods, Desal. Wat. Treat., 56 (2015) 3393–3402.
[53] S. Zhu, X. Yang, W. Yang, L. Zhang, J. Wang, M. Huo, Application of porous nickel-coated TiO_2 for the photocatalytic degradation of aqueous quinoline in an internal airlift loop reactor, Int. J. Env. Res. Pub. Healh, 9 (2012) 548.
[54] P.F. Khamaruddin, M.A. Bustam, A.A. Omar. Using Fenton's reagents for the Degradation of Diisopropanolamine: Effect of Temperature and pH, in International Conference on Environment and Industrial Innovation, Singapore, 2011.
[55] J. Herney-Ramirez, M.A. Vicente, L.M. Madeira, Heterogeneous photo-Fenton oxidation with pillared clay-based catalysts for wastewater treatment: a review, Appl. Catal., B, 98 (2010) 10–26.
[56] T. Soltani, M.H. Entezari, Solar-Fenton catalytic degradation of phenolic compounds by impure bismuth ferrite nanoparticles synthesized via ultrasound, Chem. Eng. J., 251 (2014) 207–216.
[57] N. Kashif, F. Ouyang, Parameters effect on heterogeneous photocatalysed degradation of phenol in aqueous dispersion of TiO_2, J. Environ. Sci., 21 (2009) 527–533.
[58] F.H. Al Hamedi, M.A. Rauf, S.S. Ashraf, Degradation studies of rhodamine B in the presence of UV/H_2O_2, Desalination, 239 (2009) 159–166.
[59] S. Esplugas, J. Giménez, S. Contreras, E. Pascual, M. Rodríguez, Comparison of different advanced oxidation processes for phenol degradation, Water Res., 36 (2002) 1034–1042.